Shallow Water Survey with a Miniature Synthetic Aperture Sonar

Shannon-Morgan Steele
Kraken Robotic Systems Inc.
Mount Pearl, NL, Canada
ssteele@krakenrobotics.com

Richard Charron
Kraken Robotic Systems Inc.
Mount Pearl, NL, Canada
rcharron@krakenrobotics.com

Jeremy Dillon
Kraken Robotic Systems Inc.
Mount Pearl, NL, Canada
jdillon@krakenrobotics.com

David Shea
Kraken Robotic Systems Inc.
Mount Pearl, NL, Canada
dshea@krakenrobotics.com

***Abstract*—Naval operations such as IPOE (Intelligence Preparation of Operational Environment) and explosive ordnance detection often requires high-resolution surveys in shallow water and surf zones. Surveying in such shallow water presents a variety of operational challenges. The two fundamental constraints to operating in shallow water are vehicle size and performance degradation related to environmental constraints. To effectively access shallow water, lightweight man-portable Autonomous Underwater Vehicles (AUVs) are often desired. The sonar system design and processing must also be equipped to handle the challenges of the very shallow water environment, which include sloping seabed surfaces, strong multi-path environments, and highly nonlinear vehicle motion, all of which can impair target detection and analysis. Synthetic Aperture Sonar (SAS) performance can be optimized using performance prediction models; however, currently available performance models do not sufficiently include the challenges of working in shallow water. In this paper we will develop a shallow water SAS performance model and validate the results of SAS performance from two different shallow water surveys conducted using Kraken's Miniature Synthetic Aperture Sonar (MINSAS). The results show that the MINSAS is particularly adept in shallow water conditions where its narrow vertical beamwidths and coherent integration help reject multipath and enhance target detection.**

***Index Terms*—Synthetic Aperture Sonar, Sonar Imaging, Shallow Water, Multipath**

I. Introduction

The significant propagation ranges of acoustic waves make them an excellent tool for imaging targets on the seabed. Environmental factors have a strong impact on a sonar's target detection and classification performance. Mission planning requires a comprehensive understanding of sonar performance in a wide variety of environments. Sonar performance prediction is a well researched topic; however, current performance prediction models fail to address the challenges of shallow water environments, where target detection is a high priority.

Operating in shallow water with traditional survey vessels is difficult and dangerous and thus small AUVs are desired for shallow water surveys. Man-portable AUVs are quickly becoming the platforms of choice due to their ease of handling and efficient deployment. Man-portable AUVs require miniaturized components, low power consumption, high-grade navigational sensors, and an imaging sonar capable of high area coverage rates and high resolution. Synthetic aperture sonar (SAS) is well suited to seabed survey operations because it can achieve a high area coverage rate at constant, centimeter-scale resolutions. SAS achieves these gains by coherently integrating successive pings as a small physical array moves to synthesize a larger array. SAS payloads on Man-Portable vehicles provide the operator the capability of larger vehicles, without the additional weight and handling requirements. The unique modular embodiment and compact size of Kraken's Miniature Synthetic Aperture Sonar (MINSAS) make it well suited for small man portable AUVs often used for shallow water surveys. The MINSAS can be composed of 1 to 4 receiver modules, where each module dimensions are 53×3×7 cm and weigh 6.4 kg in air. The MINSAS operates at a centre frequency of 337 kHz with a bandwidth of 40 kHz. The MINSAS produces images with 3 cm resolution in the along and across track directions.

Multipath interference in SAS data reduces the SNR and leads to reduced image contrast, impaired target detection, and degraded motion compensation performance. Many performance prediction models do not include multipath effects, or if they do, they do not consider all the multipath propagation paths. In shallow water, interference from a variety of different sources and multiple bounces can become significant, and thus must be included to accurately predict shallow water performance. Current performance prediction models also assume a flat seabed. Shallow water areas are often characterized by upward sloping seabeds. An upward sloping seabed will cause multipath to increase with range in the across track direction. In this paper, we will introduce a robust performance prediction model capable of simulating a realistic shallow water environment. To validate the new model, shallow water SAS data collected on both an AUV and Kraken's actively controlled towfish will be compared to model predictions.

II. Shallow Water Performance Prediction Model

The shallow water performance prediction model incorporates SAS gains and conditions unique to the shallow water environment into the active sonar equation (1), where SL is the source level, TL is transmission loss, NL is noise level, DI is the directivity index, and DT is the detection threshold set by the operator.

$$SL - TL + TS - NL + DI > DT \tag{1}$$

The shallow water effects included in the model are multipath, sloping seabed, and strong vehicle motion. The measured source level for the MINSAS is 210 dB. The directivity index is estimated using a model for both transmit and receive. Through the noise level term we account for ambient noise, electronic noise, and the multipath scenarios discussed in Appendix A. The ambient noise level is estimated based on the Wenz curve [1], which uses the sea state as well as the centre frequency and bandwidth of the receiver.

For this paper, the target of interest is the seabed. The performance prediction model estimates the seabed target strength using the Elastic Seabed Bottom Backscatter model described in Appendix B. We account for the the SAS gain in the target strength term. Note that for this study we are modeling the target strength of the seabed, and not an object, and thus the pulse compression gain does not need to be corrected for. The pulse compression gain does not apply to seafloor sediment because the increased echo level is exactly offset by the reduction in echo level due to the reduction in the size of the resolution cell from $\frac{CT}{2}$ to $\frac{C}{2B}$, where T is the pulse length and B is the bandwidth.

Due to coherent pulse integration, the SAS gain SG will increase the SNR at a rate expressed by (2), where D is the along track image resolution; however, the noise in the signal will also increase through pulse integration. The rate of the SG gain for the seabed and the noise is not necessarily equal. Due to the random nature of the noise in a given pulse, the noise level will experience a gain (SG_N) at the rate of (3) and thus this gain must be accounted for in the model [2].

$$SG = 10\log_{10}\left(\frac{L_{SAS}}{D}\right) \tag{2}$$

$$SG_N = 10\log_{10}\left(\sqrt{\frac{L_{SAS}}{D}}\right) \tag{3}$$

III. Test Data

A. Study Area 1: Lake Ontario

In September 2017, Kraken conducted surveys in Lake Ontario in search of AVRO Arrow models. Sonar imagery was collected with Kraken's MINSAS60 (single receiver module per side) onboard the Kraken ThunderFish AUV. The MINSAS was operated at a pulse repetition interval of 0.135 s with a pulse length of 1 ms. During this survey the sea state was one and the wind speed was negligible. Since Lake Ontario is a freshwater lake, the salinity was assumed to be zero. The water temperature was 20°C. Previous geologic surveys of the region indicate that the bottom is composed of bedrock [3]. The bottom slope is 0.3% up towards shore.

We analyze both the port and starboard data from two legs of the survey, collected in opposite directions approximately 1.5 km away from shore, in approximately 6.5 m water depth at an altitude of 5 m. The leg spacing is 50 m apart, and thus there was significant overlap in the survey data. This data set was chosen as an example because in all four data sets there is a strong and obvious multipath interference occurring at long range (Fig. 1 & 2).

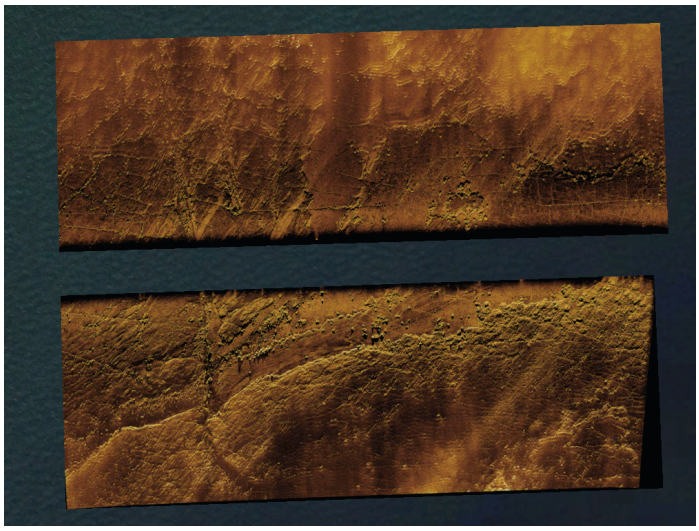

Fig. 1. Google Earth image overlaid with port and starboard SAS mosaics collected during leg 1 of the Lake Ontario data set.

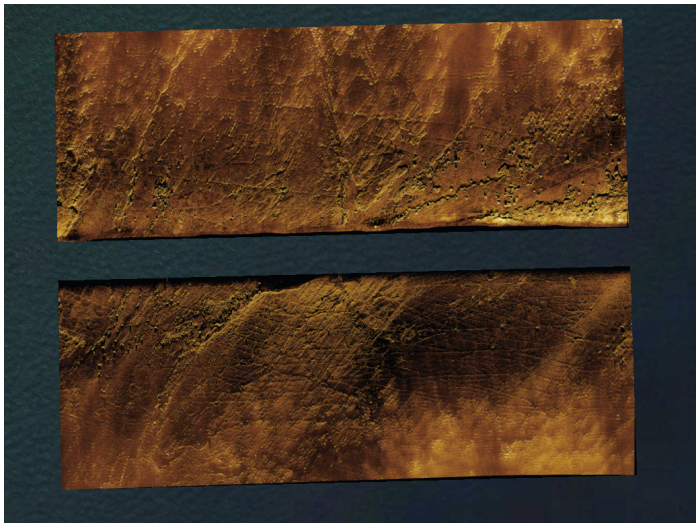

Fig. 2. Google Earth image overlaid with port and starboard SAS mosaics collected during leg 2 of the Lake Ontario data set.

B. Study Area 2: Holyrood, NL

In June 2018, Kraken took part in the Shallow Water Survey as part of the 8th International Conference on High Resolution Surveys in Shallow Water. For this survey, Kraken utilized the KATFISH actively controlled towfish equipped with the MINSAS180 (three receiver modules per side). The KATFISH was towed by the 43 ft long vessel MV Predator. The survey was conducted in Conception Bay, near Holyrood, Newfoundland, Canada. The MINSAS was operated at a pulse repetition interval of 0.21 s with a pulse length of 1 ms. The average tow speed of the KATFISH was 5.5 knots and the average altitude above the seabed was 12 m. The wind speed

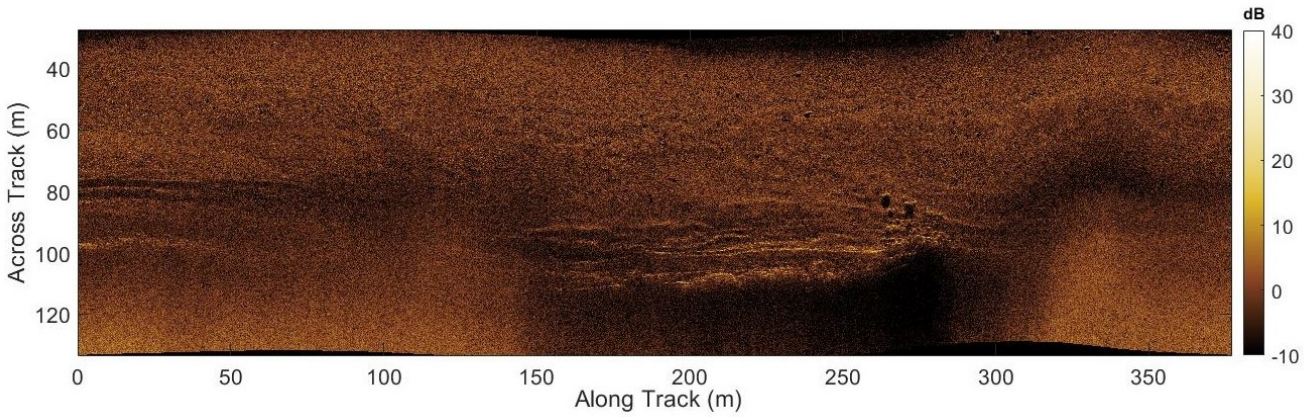

Fig. 3. SAS mosaic of shallow water data collected in Holyrood.

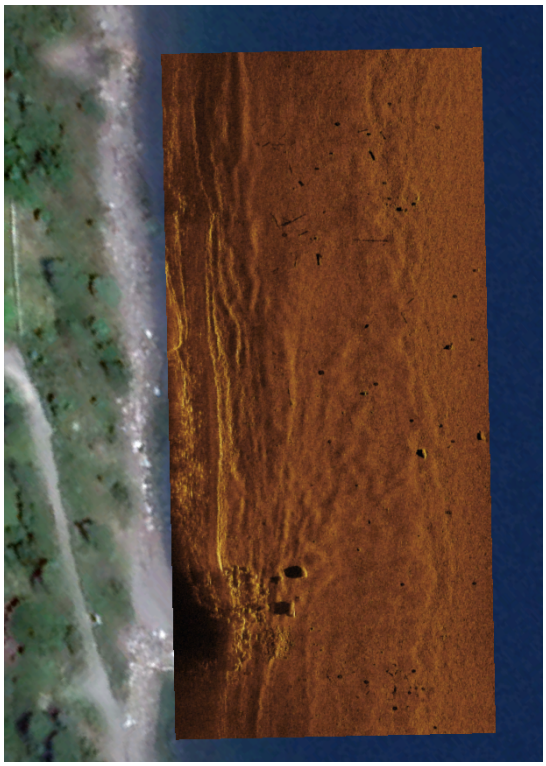

Fig. 4. Google earth image overlayed with cropped Holyrood SAS Mosaic.

during this survey was 15 knots and the sea state was three. The water temperature was 7°C. The survey area average water depth was 17 m with a 16% seabed slope.

In addition to sloping seabeds and multipath, the Holyrood survey environment was particularly challenging due to internal waves, large schools of fish, and sound velocity changes due to freshwater runoff. Samples of the seabed sediment were not collected. The sediment is therefore assumed to be a medium sand. Despite these challenges the Holyrood SAS data is an excellent data set for validating the shallow water SAS performance model because there are areas where the SNR can be observed to drop below zero (Fig. 3), as well as areas where the sonar was able to image right up to the shoreline (Fig. 4), depending on the roll angle of the towfish.

IV. Model-Data Comparison

The Shallow Water SAS performance model was verified by comparing the range-dependent SNR predicted by the model to the measured range-dependent SNR, averaged over multiple pings. The MINSAS is able to measure the SNR indirectly using the vertically offset arrays used to measure bathymetry. The SNR at each range of interest $\sigma(r)$ can be calculated as

$$\sigma(r) = \frac{c(r)}{1 - c(r)} \tag{4}$$

where $c(r)$ is the normalized cross-correlation of the signals between the two vertically separated arrays.

A. Study Area 1: Lake Ontario

Since the motion and environmental parameters do not vary significantly in the along track direction for each leg, the SNR as a function of range was averaged over the entire image for both port and starboard.

The modeled and measured SNR agree quite well in both the port and starboard directions, with a majority of the errors being less than 5 dB (Fig. 5, 6, 7, and 8). The slope in this area is low and thus does not contribute significantly to the difference in SNR performance when comparing up slope and downslope SNR. In this case, it is primarily the roll of the AUV that caused differences in the range performance between images. The average measured roll was 1.5 and 2° for leg 1 and 2, respectively, causing differences in port and starboard depression angles of 3 to 4°. The MINSAS is mounted on the vehicle at a depression angle of 10°, so for leg 1 the depression angle was rolled up to 8.5° on starboard and down to 11.5° on port. This causes the leg 1 starboard (Fig. 5) to have a higher SNR at the far ranges than the port data (Fig. 6). During leg 2 depression angle was rolled up to 8° on starboard and down to 12° on port, causing the starboard (Fig. 7) data to once again have higher SNR than the port side (Fig. 8) at far range.

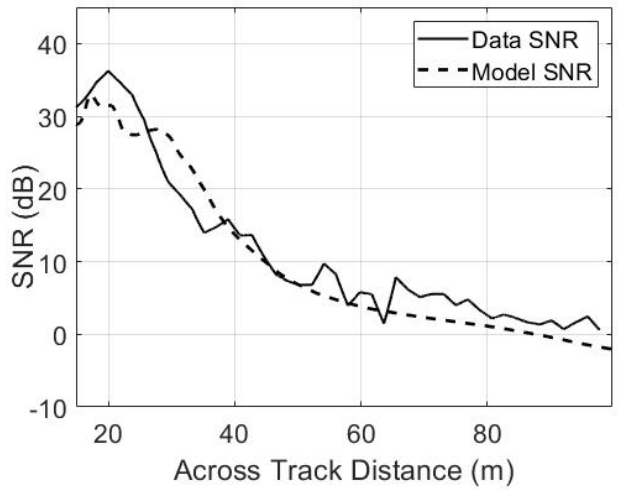

Fig. 5. Comparison of measured and modeled SNR for leg 1, starboard side.

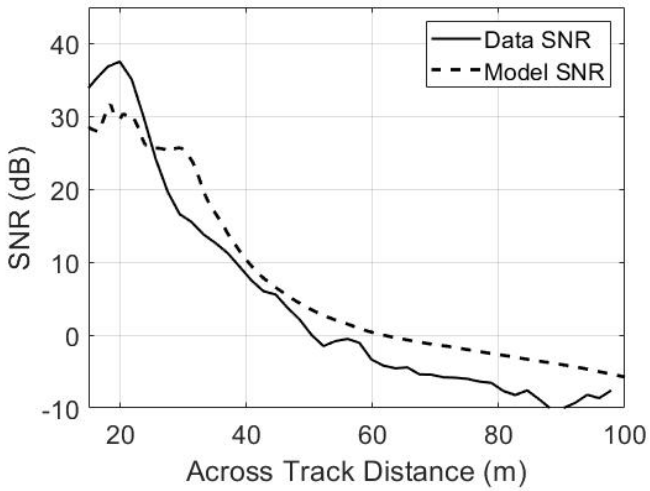

Fig. 6. Comparison of measured and modeled SNR for leg 1, port side.

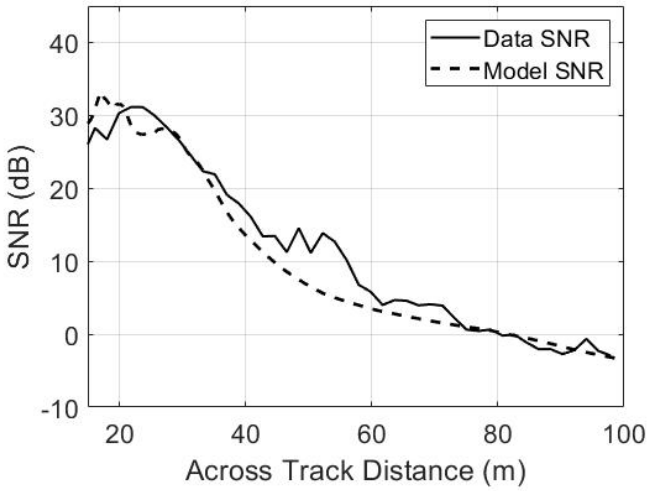

Fig. 7. Comparison of measured and modeled SNR for leg 2, starboard side.

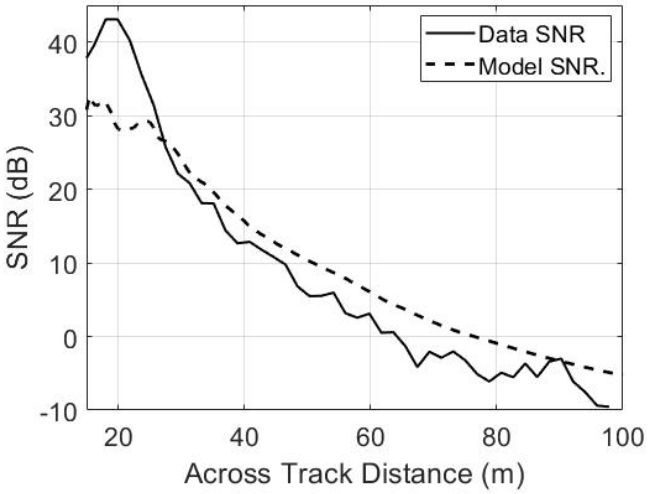

Fig. 8. Comparison of measured and modeled SNR for leg 2, port side.

B. Study Area 2: Holyrood, NL

The Holyrood area has considerable motion variation in the along track direction, with the most significant motion being roll. Based on the measured roll (Fig. 9), the image will be divided into three different sections to be averaged over 20 pings and compared to their corresponding model. The three sections are centered at 100 m (2.5° roll), 240 m (−2.4° roll), and 332 m (5° roll). Since the Holyrood data was collected on the starboard side, a negative roll corresponds to a decreased depression angle and thus we should expect improved range performance at the 240 m location.

At the 100 m along track position the model is able to predict the sonar performance reasonably well, with most errors less than 5 dB. Except for at near range, where the error is quite significant, possibly due to imperfect beampattern inversion, changing seabed slope, or sediment type variation. The model is able to accurately predict that at 100 m the sonar is no longer recording signal from the seabed due to the roll geometry. This appears in the measured SNR data as an SNR low-point, followed by a slight increase as SNR due to the signal becoming dominated by noise.

At the 240 m along track position, we see that, as predicted, the SNR is much higher at range in this region of the image because of the reduced depression angle. As with the 100 m data, we see a large difference between the model and data SNR at near range. At far range we observe strong agreement between the model and the data SNR, with most errors less than 3 dB.

At the 332 m along track position we find significant variation between the model and the data. This variation is likely due to the high instability of the towfish in this region. Although we have attempted to account for roll, we did not account for any of the other motion in the model. It is also

possible that with such a high roll (5°), we are starting to go into a region where sidelobes become significant, causing interference in the data as well as inaccurate beampattern inversion. It should also be noted that the model does not include some of the other challenges experienced during the Holyrood survey such as internal waves and water column interference (schools of fish), both of which could alter the measured SNR and could be of interest for future work.

V. Conclusion

In this paper we introduced a new shallow water SAS performance prediction model that incorporates the shallow water environment conditions not previously included in sonar performance models. The model was also expanded to include the vertical beampatterns and coherent processing that make the MINSAS effective in shallow water. The new shallow water performance prediction model has been validated using two different shallow water data sets. In the very shallow regime (6.5 m water depth) and benign slope environment of Lake Ontario, the model was able to accurately predict the SNR as a function of range. Given the large amount of uncertainty of the environmental conditions in Holyrood, the model was able to predict the sonar performance well. The Holyrood environment is likely more complicated than what our current model simulates. There may be varying sediment types and non-linear slope, both of which could be incorporated into the model in the future. Nevertheless, the model correctly predicted changes in multipath performance due to towfish roll angle. Improved beampattern inversion may also be required for high instability conditions and should be a topic of future work.

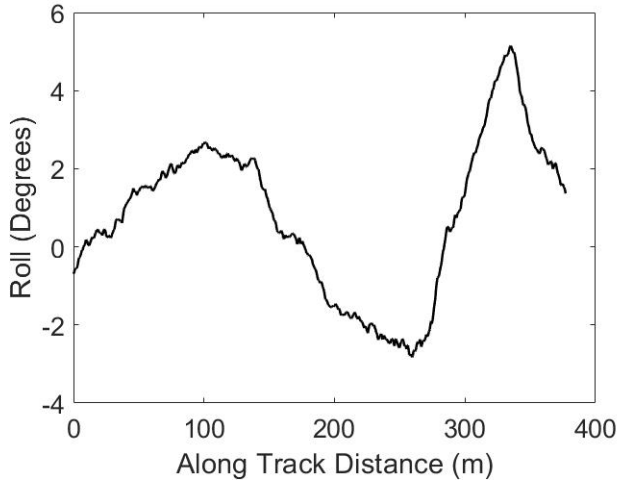

Fig. 9. Measured roll as a function of along track distance.

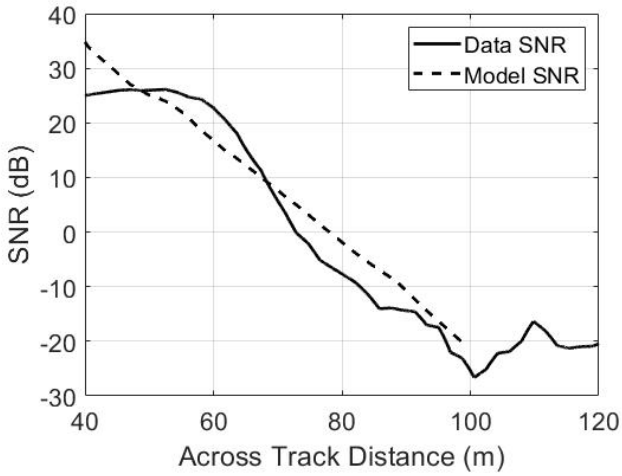

Fig. 10. Comparison of modeled and measured average SNR for 2.5° roll location.

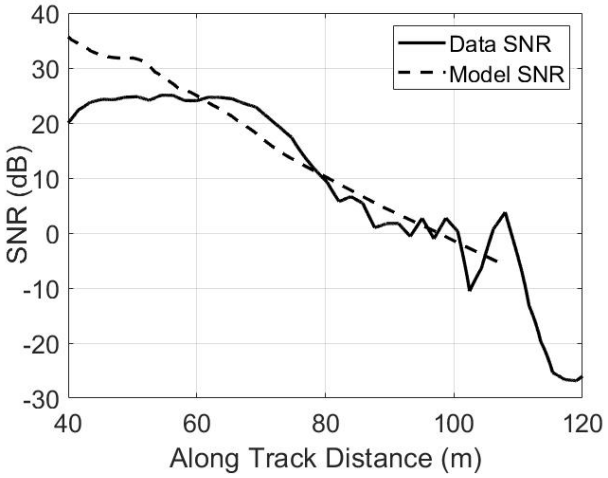

Fig. 11. Comparison of modeled and measured average SNR for −2.5° roll location.

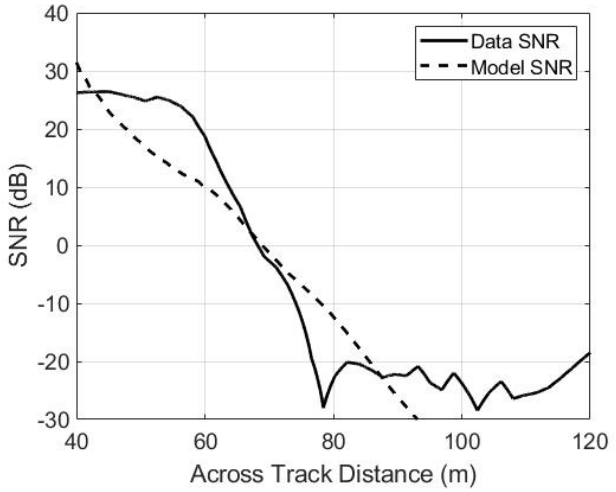

Fig. 12. Comparison of modeled and measured average SNR for −2.5° roll location.

APPENDIX A
MULTIPATH SCENARIOS

1) Direct sea surface return
2) From projector, to seabed, to sea surface, and back to hydrophone
3) From projector, to sea surface, to seabed, and back to hydrophone (reverse of 2)
4) From projector, to sea surface, to seabed, back to sea surface, and back to hydrophone
5) From projector, to seabed, backscattered to sea surface, reflected to seabed, and forward scattered to hydrophone
6) From projector, to seabed, forward scattered to sea surface, reflected to seabed, and backscattered to hydrophone (reverse of 5)

APPENDIX B
ELASTIC SEABED BOTTOM BACKSCATTER

This model is an updated version [4] of the APL-UW backscattering model [5]. The model includes contributions from the sediment interface roughness and volume scattering. For roughness scattering, the model uses the small-slope formalism of [6], adapted to elastic seafloors [7], [8]. For seafloor volume scattering, the elastic perturbation approximation [9]–[11] is used. The input parameters used to generate the medium sand and silt sediments demonstrated in this paper can be found in [4].

REFERENCES

[1] G. M. Wenz, "Acoustic ambient noise in the ocean: Spectra and sources," *The Journal of the Acoustical Society of America*, vol. 34, no. 12, p. 19361956, 1962.

[2] J. I. Marcum, *A Statistical Theory of Target Detection By Pulsed Radar*, 1952.

[3] N. A. Rukavina, "Nearshore sediments of lakes ontario and erie," *Geoscience Canada*, vol. 3, no. 3, pp. 185–190, Aug 1976.

[4] D. Jackson, *High-Frequency Bistatic Scattering Model for Elastic Seafloors*. University of Washington Seattle Applied Physics Lab, 2000.

[5] U. of Washington, *APL-UW High-Frequency Ocean Environmental Acoustic Models Handbook*, 1994.

[6] A. G. Voronovich, "Wave scattering from rough surfaces," *Springer Series on Wave Phenomena*, 1994.

[7] T. Yang and S. L. Broschat, "Acoustic scattering from a fluid-elastic-solid interface using the small slope approximation," *The Journal of the Acoustical Society of America*, vol. 96, no. 3, pp. 1796–1804, 1994.

[8] D. Wurmser, "A manifestly reciprocal theory of scattering in the presence of elastic media," *Journal of Mathematical Physics*, vol. 37, no. 9, pp. 4434–4479, 1996.

[9] A. Ivakin, "Sound scattering by inhomogeneities of an elastic half-space," *Soviet Physics Acoustics*, vol. 36, pp. 377–380, 07 1990.

[10] A. N. Ivakin and D. R. Jackson, "Effects of shear elasticity on sea bed scattering: Numerical examples," *The Journal of the Acoustical Society of America*, vol. 103, no. 1, pp. 346–354, 1998.

[11] D. R. Jackson and A. N. Ivakin, "Scattering from elastic sea beds: First-order theory," *The Journal of the Acoustical Society of America*, vol. 103, no. 1, pp. 336–345, 1998.